

Inhomogeneity in the Hot Intracluster Medium of Abell 1060 Observed with Chandra

Akira HAYAKAWA¹, Tae FURUSHO², Noriko Y. YAMASAKI², Manabu ISHIDA¹, and Takaya OHASHI¹

¹*Department of Physics, Tokyo Metropolitan University,*

1-1 Minami-Ohsawa, Hachioji, Tokyo 192-0397

²*Institute of Space and Astronautical Science, Japan Aerospace Exploration Agency,*

3-1-1 Yoshinodai, Sagamihara, Kanagawa 229-8510

E-mail(AH): akira.h@phys.metro-u.ac.jp

(Received 2004 June 11; accepted 2004 August 3)

Abstract

A Chandra observation of the non-cooling flow cluster A 1060 has confirmed that the hot intracluster medium has fairly uniform distributions of temperature and metal abundance from a radius of about 230 kpc to the central 5 kpc region ($H_0 = 75 \text{ km s}^{-1} \text{ Mpc}^{-1}$). The radial temperature profile shows a broad peak at 30–40 kpc from the center at a level $\sim 20\%$ higher than that in the outer region. Assuming spatially uniform temperature and abundance distributions, we derived a 3-dimensional density structure by iteratively correcting the β model, and obtained the central gas density to be $8.2_{-1.0}^{+1.8} \times 10^{-3} \text{ cm}^{-3}$. The distribution of gravitational mass was estimated from the density profile, and a central concentration of mass within a radius of 50 kpc was indicated. The data also suggest several high-abundance regions. The most significant blob adjacent to the central galaxy NGC 3311 has a radius of about 9 kpc, which indicates a metallicity of ~ 1.5 solar. We consider that this blob may be produced by the gas stripped off from NGC 3311.

Key words: galaxies: clusters: individual (Abell 1060) — galaxies: intergalactic medium — X-rays: galaxies

1. Introduction

The spatial distributions of the temperature and metallicity in the intracluster medium (ICM) tell us about the past history of cluster formation and the metal-enrichment process. In the cores of relaxed clusters, recent studies from Chandra and XMM-Newton observatories have revealed various interesting features. Regarding the temperature structure, the observed absence of very cool gas at the center strongly requires some heat-injection mechanism (e.g. Peterson et al. 2003), which is not yet understood very well. A close study of a system without any significant cooling flow may give new insight into these problems. Another important aspect of the non-cooling-flow system is a reliable estimation of the gravitational mass profile, based on a fairly uniform temperature distribution. Such an attempt was carried out for NGC 1399 (Ikebe et al. 1996), NGC 4636 (Matsushita et al. 1998), and A 1060 (Tamura et al. 2000), and a mass concentration within a radius 20–40 kpc has been recognized.

As for the metallicity distribution, significant radial gradients are seen mainly in cD clusters, characterized by a metal concentration at the center. It is discussed that the central excess in the metal abundance is likely to be created by a bright central galaxy (De Grandi et al. 2004). Since the metal accumulation, due to a type Ia supernova and stellar mass loss, takes 2–10 Gyr, the central regions need to be undisturbed for a long time (Böhringer et al. 2004). Using recent high-resolution data,

the abundance rise at the center has been shown to often accompany a sharp drop right at the cluster center within $r < 10$ –30 kpc (Perseus: Schmidt et al. 2002; Sanders et al. 2004; Centaurus: Sanders and Fabian 2002; 0335+096: Mazzotta et al. 2003; A 2052: Blanton et al. 2003; and A 2199: Johnstone et al. 2002). A projection effect of a multi-temperature gas is discussed as being a part of the cause (Molendi and Gastaldello 2001), while in some systems abundance depletion seems to be a real feature. A two-dimensional metallicity distribution was first studied using the ASCA data for Centaurus cluster and 2A 0335+098, which indicated a patchy distribution of iron (e.g. Tanaka et al. 2003). A Chandra observation of a cluster around 4C +55.16 showed an unusual iron-rich plume (Iwasawa et al. 2001), and AWM 7 (Furusho et al. 2003) revealed a blob-like metal concentration with a size 0.3–1 kpc near the center. Therefore, metal injection from the central galaxy may take place in a highly inhomogeneous way.

To further understand the ICM properties and metal-injection process, a detailed study of non-cD type clusters is useful. By comparing the metallicity feature, we can separate the effect of cD galaxies and estimate how central enrichment proceeded. A nearby cluster of galaxies, A 1060 ($z = 0.0114$), is known to have no cool or sharp X-ray peak at the center, and its proximity and brightness enable us to evaluate the detailed temperature structure and iron distribution in the central region. The cluster has 2 giant elliptical galaxies, whose X-ray emissions were

found to be very compact (Yamasaki et al. 2002), which helps us separate the ICM emission easily. Also, the temperature in this cluster is very uniform with little sign of a cool component (Furusho et al. 2001). This leaves little systematic ambiguity in estimating the iron abundance simply from the equivalent width.

The Chandra results on the 2 giant elliptical galaxies (NGC 3311 and NGC 3309) near the center of A 1060 were reported in Yamasaki et al. (2002). The present paper deals with the distributions of the temperature and metallicity in the central ICM in some detail. Preliminary results were given in Furusho et al. (2002). We assume $H_0 = 75 \text{ km s}^{-1} \text{ Mpc}^{-1}$ with $q_0 = 0.5$, and an angular size of $1'$ corresponding to 13 kpc. The solar number abundance of Fe relative to H is taken as 4.68×10^{-5} (Anders and Grevesse 1989). We employ Galactic absorption as $N_{\text{H}} = 6 \times 10^{20} \text{ cm}^{-2}$ throughout the paper.

2. Observation and Analysis

The Chandra observation of A 1060 was carried out on 2001 June 4, with ACIS-I, for a total exposure time of 32 ks in the Very Faint Mode. The CIAO ver 3.0 package was used in the data reduction and a calculation of the energy response. We generated background images and spectra based on blank-sky data and software prepared by Maxim Markevitch.¹ For a spectral fitting, XSPEC ver 11.2.0 was used, and because of a known problem of the ACIS response below 1 keV, we added the ACISABS absorption model available in XSPEC.

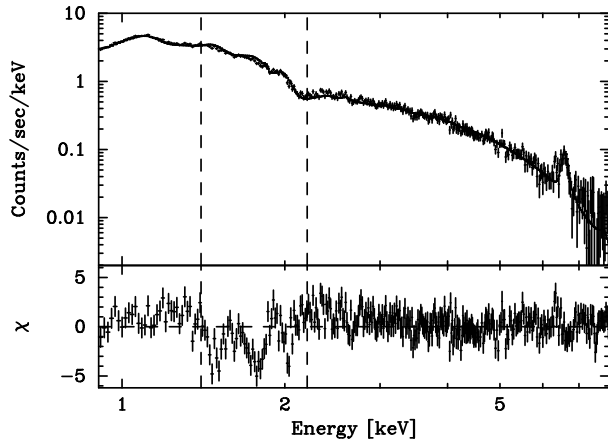


Fig. 1. X-ray Spectrum of A 1060 for the sum of the 4 ACIS-I chips. The data were fitted with a MEKAL thermal model with interstellar and ACISABS absorptions. The bottom panel shows the residuals of the fit. The model fit has a problem in the energy range 1.4–2.2 keV, which was excluded in the spectral analysis.

Before proceeding to spatially resolved spectroscopy (subsection 4.3), we fit the overall cluster spectrum to look at the consistency with the previous results. Figure 1 shows the spectrum between 0.9 and 8.0 keV from the entire ACIS-I chips fitted by a single-temperature MEKAL

model, including Galactic N_{H} and ACISABS absorption. A large deviation from the model, which might be due to a calibration uncertainty of the Ir edge of the X-ray mirror, is seen in the energy range 1.4–2.2 keV as being bounded by dashed lines. By masking this region, the fit was improved from $\chi^2/\nu = 732/361$ to $\chi^2/\nu = 385/305$. Therefore, we do not include this region in a later spectral analysis. The obtained spectral parameters for the temperature and metal abundance are $kT = 3.36^{+0.05}_{-0.06} \text{ keV}$ and $Z = 0.33^{+0.03}_{-0.03} \text{ solar}$, respectively. They are in reasonable agreement with the values from EXOSAT ($3.3^{+0.4}_{-0.3} \text{ keV}$ and $< 0.46 \text{ solar}$ by Edge and Stewart 1991) and ASCA ($3.24 \pm 0.06 \text{ keV}$ and $0.30 \pm 0.02 \text{ solar}$ by Fukazawa et al. 1998).

3. X-Ray Image

The X-ray intensity contours obtained with ACIS-I are overlaid on the optical image in figure 2a. The data are for the energy range 0.9–8.0 keV, and have been corrected for vignetting and adaptively smoothed by a Gaussian function with a 1σ width of $2''$. Except for the 2 peaks corresponding to the bright central galaxies, NGC 3311 and NGC 3309 as shown in Yamasaki et al. (2002), the ICM in A 1060 is very smooth and devoid of any prominent spatial structures. This is in a marked contrast to the X-ray filaments and cavities that are clearly recognized in the Chandra images of cD-type clusters.

As can be seen in the expanded X-ray image in figure 2b, there is a small extended emission apparently trailing in the northeast direction from NGC 3311 with an angular scale $\lesssim 1'$. We examined whether this excess feature might correspond to the potential minimum of the cluster. The center of the cluster-wide X-ray emission can be estimated from ROSAT data, which covers a diameter of $\sim 2^\circ$. A two-dimensional fit for the ROSAT data, excluding the central two galaxies, indicate that the center of the ICM emission is $28''$ southwest of NGC 3311, opposite to the direction of the excess emission. This suggests that the excess X-ray emission could be related to the elliptical galaxy NGC 3311. However, since many clusters show their X-ray peaks offset from the isophotal centroid, there remains a possibility that the feature in the northwest of NGC 3311 corresponds to the minimum of the gravitational potential.

Figure 2b also shows a weak source at $30''$ south of NGC 3311, which is inside the isophotal radius ($95''$) of NGC 3311. Although the nearest known source is a globular cluster SGM95 33, it is $2''$ offset from the X-ray position, and is unlikely to be the counterpart.

4. Radial Profiles

4.1. Temperature and Metal Abundance

The radial distributions of the ICM temperature and metallicity were examined. The two central galaxies (for NGC 3311, $r \sim 20''$, for NGC 3311, $r \sim 15''$) and other point sources (twice as large as the detected radius based on CIAO wavelet and cell detection tools) were excluded.

¹ <http://hea-www.harvard.edu/~maxim/axaf/acisbg/>.

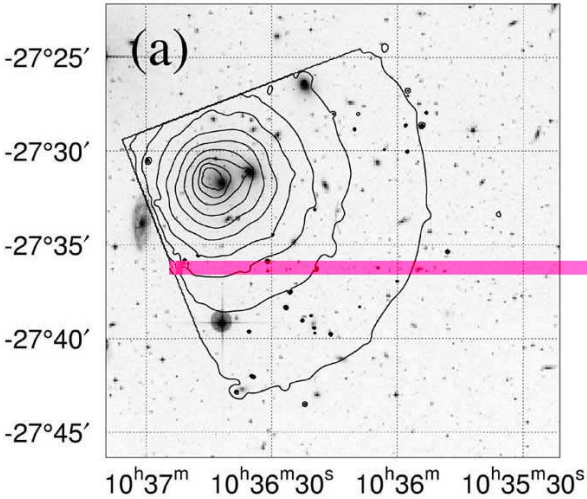


Fig. 2. (a) Optical image of A 1060 taken from the Digitized Sky Survey. The overlaid contours show a smoothed X-ray image. (b) Expanded X-ray image of the $5' \times 5'$ region centered on A 1060. The crosses show the positions of NGC 3311 (center) and NGC 3309 (north-west by $2'$), respectively.

The annular spectral data for radii $r > 20''$ were accumulated in concentric annular regions by keeping the number of photons greater than 10000 in each annulus. Figure 3 shows the radial distributions of the temperature, metal abundance, and the χ^2 value for the spectral fit by absorbed MEKAL models. The bottom panel indicates that a single-temperature thermal model gives a reasonably good fit with reduced χ^2 values less than 1.4 in all of the regions.

As can be seen in figure 3, the temperature shows a rise up to about 3.7 keV at $r = 2'-3'$ from the center. This feature is significant, and a hypothesis of a constant temperature over the whole radius is rejected with more than the 90% confidence. The highest temperature (~ 3.7 keV) exceeds the level in the outer region by about 20%. In the X-ray image, however, there is no clear structure or

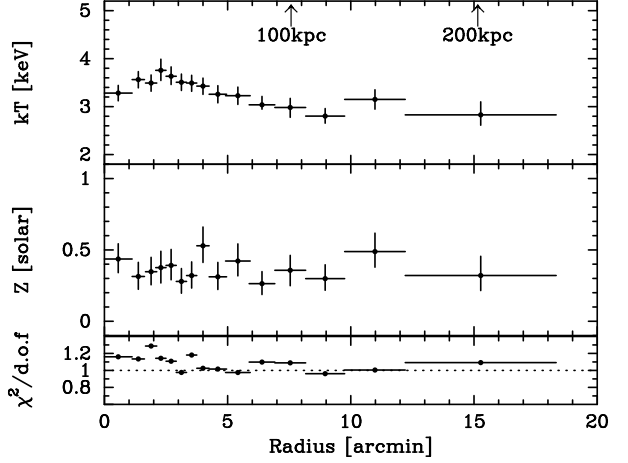


Fig. 3. Radial distribution of the temperature (top), metal abundance (middle), and the χ^2 value of the spectral fit (bottom), based on a spectral fit for concentric annular regions. The errors are single-parameter 90% limits.

edge-like feature at this radius. We also note that the central temperature of about 3.4 keV is much higher than those seen in so-called cooling flow clusters, which generally show a temperature drop down to 1/2–1/3 of the outer level. Therefore, gas cooling is certainly not a major process occurring at the center of A 1060. In the outward direction, the temperature gradually declines from $r = 2'$ to $8'$ by more than 0.5 keV in a monotonic way. Since the ICM temperature in the outer region ($r \sim 30'$) measured with ASCA is about 3.0 keV (Furusho et al. 2001), the temperature gradient is confined only in the central region ($r < 8'$ or 100 kpc).

The metal abundance in figure 3 is consistent with the overall value of 0.33 solar in all regions. The innermost region ($r < 1'$) suggests a somewhat high value of $0.44^{+0.11}_{-0.10}$ solar, but no systematic rise toward the center, as seen in other cD-type clusters, is recognized. The constant metallicity and the observed value are consistent with the previous ASCA result (Furusho et al. 2001; Tamura et al. 2000).

4.2. Density Profile

We plot the surface brightness profile in the energy range 0.9–8.0 keV in figure 4. The blank-sky data were subtracted in this plot. The data were fitted with a single β model, but the fit is not acceptable because of a discrepancy in the central region. The data seem to require an additional narrow component. Although a double β model is often used to fit the data, the superposition of 2 separate emission components is physically difficult to interpret. We explored a solution of a 3-dimensional density structure with a single emission component based on the assumption that the temperature and metallicity are constant with radius, and also that the cluster is spherically symmetric, which seem to be a reasonable approximation of the observed features.

We first excluded the central region, and only fitted data in the outer region ($r = 4'-18'$), which gave an ac-

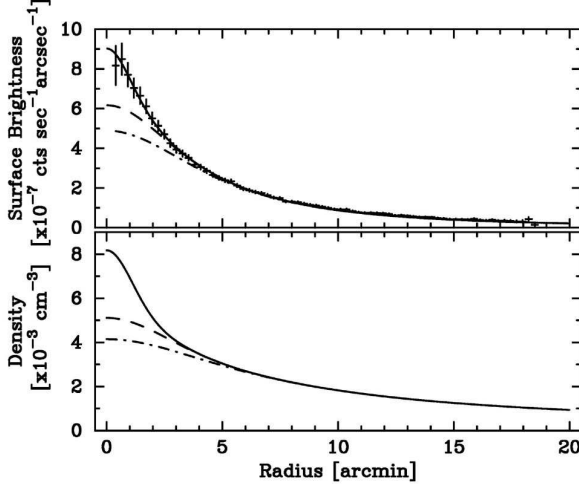


Fig. 4. Radial distribution of the surface brightness (top) and density (bottom). The data points are indicated by crosses, in which point sources and the central two galaxies are subtracted. The model approaches the observed data by iteratively enhancing the central density. The 3 lines correspond to the initial (β model, dash-dotted line), the 2nd (dashed line), and the 7th (solid line) iterations, respectively.

ceptable fit (the bottom dash-dot curve in figure 4). The fitted parameters are $r_c = 5.5^{+1.4'}_{-1.3'}$ and $\beta = 0.56^{+0.07}_{-0.05}$, respectively. We then tried to modify the radial density profile within $r \leq 4'$ from the β model, and found an acceptable one that gives a surface brightness profile consistent with the observed data. To find the best estimate of the density profile, we performed an iteration in the following way.

We took the ratio between the surface brightness (Σ) data and the single β model, which is about 1.8 at the center, and drops to unity at $r = 4'$. Since the emissivity scales as the square of the density, we took the square root of the brightness ratio, i.e. $\eta = \sqrt{\Sigma_{\text{data}}/\Sigma_{\beta}}$, which varies as a function of the radius, and used it as a correction factor to the β -model density. The β -model density profile was multiplied by η , and the predicted brightness profile was compared with the data. In this process, the ratio as a function of the radius was approximated by the sum of a Gaussian function and a constant, which was found to give a good fit to the observed profile.

The brightness and density profiles at this stage are shown by the 2nd curves from the bottom (dashed) in the top and bottom panels of figure 4. The resultant brightness profile became steeper than the pure β case, but not as sharp as the data, because our correction factor is “diluted” by the emission in the cluster outskirts superposed in the line of sight. This corrected β model was replaced by the previous β model, and we took the ratio of the surface brightness again and calculated further correction factors in the same manner for each radius. This iteration process was ended when the brightness profile gave an acceptable χ^2 value to fit the data. This took 7 iteration steps. The resultant profile is shown in the top curve (solid) of figure 4. The 3-dimensional density profile now shows

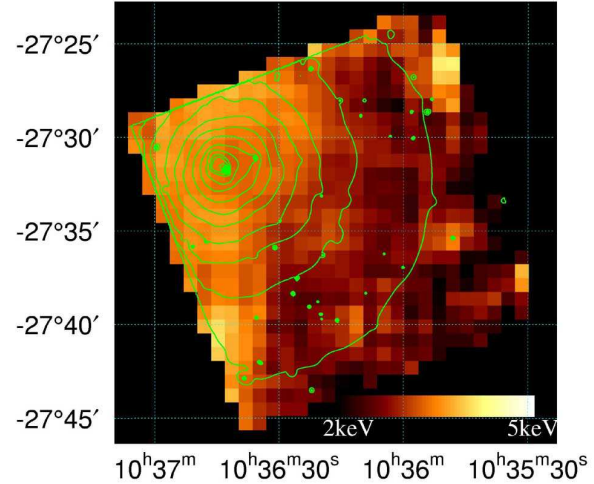


Fig. 5. Temperature map obtained from the hardness ratios. The pixel size is $44'' \times 44''$ (10 kpc across). The color coding was performed for a temperature range $kT = 2\text{--}5$ keV. The X-ray intensity contours are the same as in figure 2a.

a fairly sharp peak in the center, with a density about twice as much as that of the β model (top solid curve in the bottom panel of figure 4). We use this density profile in a later estimation of the physical parameters in the core region. The central electron density estimated here is

$$n_0 = 8.2^{+1.8}_{-1.0} \times 10^{-3} \text{ cm}^{-3},$$

which is still lower than the level in other cD-type clusters.

5. Spatial Distribution

5.1. Temperature Distribution

ASCA observations have shown that the ICM of A 1060 was very isothermal (Tamura et al. 2000; Furusho et al. 2001). However, the angular resolution of ASCA did not allow us to look into the temperature structure on spatial scales less than a few arcmin. Here, we examine the temperature structure within $r < 20'$ from the center based on the Chandra data. The hardness ratio (HR) was calculated for two energy bands, 2–6 keV and 0.9–2 keV, after a point-source elimination and background subtraction. Regions containing NGC 3311 and NGC 3309 were masked out with a diameter of 1'. We assumed a single-temperature MEKAL model with a metal abundance of 0.3 solar absorbed with Galactic N_{H} and ACISABS.

The absence of an intense soft component and the constancy of the metal abundance in A 1060 assures us that the HR values are reliable measures of the temperature. The effect of a metallicity variation on the derived HR values is fairly small. A change of the metal abundance from 0.3 to 0.5 solar in the model results in a temperature shift of 0.06 keV (less than the statistical error of about 0.1 keV) from the nominal level of 3 keV.

Figure 5 shows a color-coded temperature map obtained from the HR distribution. The statistical error in the temperature is typically 0.3 keV (1σ) at $r \sim 5'$. The pixel

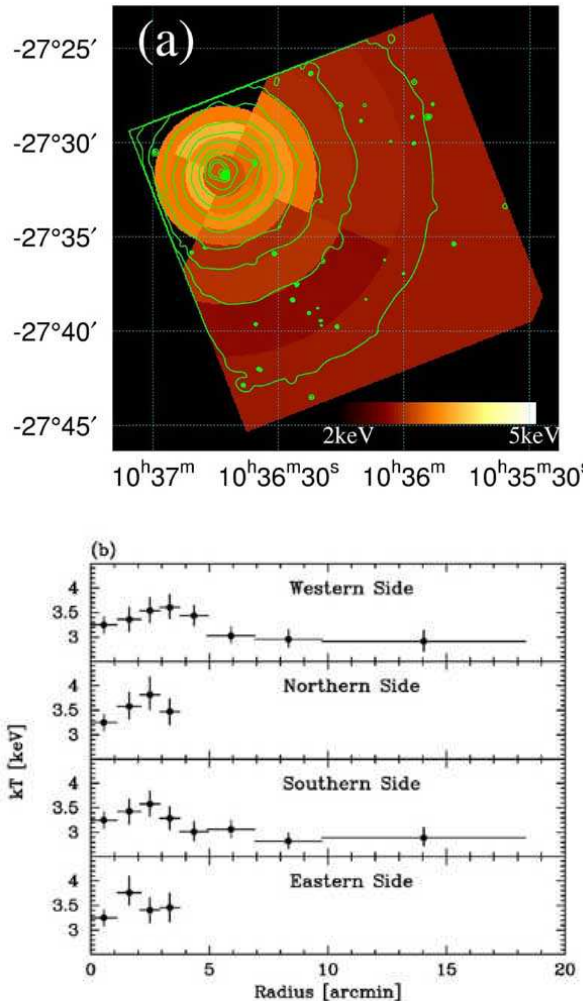


Fig. 6. (a) Temperature map obtained from spectral fits. (b) Radial temperature profiles for 4 directions, based on the results shown in (a)

size is $44'' \times 44''$ (10 kpc across), and we took a running average for the HR over 4×4 pixels. The map confirms the general trend that the temperature in the outer region is cooler than the cluster center. Also, the region around $r \sim 3'$ appears to be hotter than at the exact center, which is consistent with the radial temperature profile in figure 3. We also note that the warm ring at $r \sim 3'$ shows no clear azimuthal structure, and that the variation of the temperature looks fairly gradual in all regions.

To confirm the temperature distribution indicated by the hardness ratio analysis, we performed spectral fits by accumulating data in larger regions. For 8 radially divided annuli, we further limit their opening angles to 90° . The spectral data were accumulated, background-subtracted, and fitted with a single-temperature MEKAL model. The absorption was fixed to the Galactic value, and the metal abundance fixed to 0.3 solar. We thus obtained the temperature map shown in figure 6a. The similarity with figure 5 is quite evident, and the result confirms the relatively small variation of temperature in this cluster. The

temperature in the outermost ($r > 10'$) large region is 2.9 keV, which is significantly cooler than the level in the central region. The temperature values are also plotted in figure 6b as a function of the radius for 4 different azimuthal directions. Here, we confirm that the temperature shows a broad peak at $r \sim 3'$ in all directions. There is no significant difference in the 4 profiles.

5.2. Metal Distribution

The isothermal ICM of A 1060 helps us look into the metallicity (iron in particular) distribution in a straightforward way. Since the equivalent width of the Fe-K line changes by about 10% for a temperature change of 1 keV at $kT \sim 3$ keV, the constant temperature ($\Delta T < 0.3$ keV) suppresses the systematic ambiguity in determining the metallicity. To estimate the Fe abundance distribution, we took the HR between energy bands 6–7 keV and 2.2–6 keV. The hard band contains the Fe-K emission line at 6.7 keV (redshifted to 6.62 keV), and the fraction of the line photon is about 10% for a 3 keV plasma containing 0.3 solar abundance of iron. The soft band is devoid of any prominent line, such as those of Si, and the intensity is a good measure of the continuum level. In fact, changing the metal abundance from 0.3 to 0.5 solar at $kT = 3$ keV pushes up the 2–6 keV flux by only $\sim 6\%$. These features indicate that the HR for these 2 energy bands is a good measure of the iron abundance.

The ratios were calculated for the background-subtracted data. The spatial distribution of the HRs are shown in figure 7a as a color-coded map, in which the data are accumulated in $22'' \times 22''$ pixels. In this plot, the HR values were converted to iron abundance assuming a constant temperature of $kT = 3.0$ keV. The statistical error on the abundance is typically ± 0.1 solar everywhere. We notice that there are some regions with high metallicity in this hardness map. These regions are numbered and marked with circles. In the HR values, their statistical significances are between 1.7σ and 2.5σ . Since the number of pixels in $r < 5'$ is about 500, it is unlikely that these deviations are due to statistical fluctuation.

To raise the statistical quality of the HRs in the outer regions, the data were further binned in $88'' \times 88''$ pixels, and the corresponding temperatures are plotted in figure 7b. There are some high abundance regions seen in the northwest edge. The statistical significance is $\sim 2.5\sigma$. Apart from these high-abundance patches near the field edge, the values seem to be fairly constant in a wide region with $r = 3'-10'$.

Again, we carried out a spectral analysis for the segmented regions, and the results on the metal abundance are shown in figure 8a. Even though most of the notable structures are smoothed out, the results are generally consistent with the HR results shown in figures 7a and b. We also note that there is no systematic drop or rise as a function of the radius in the abundance feature. The same results are plotted in figure 8b as a function of the radius.

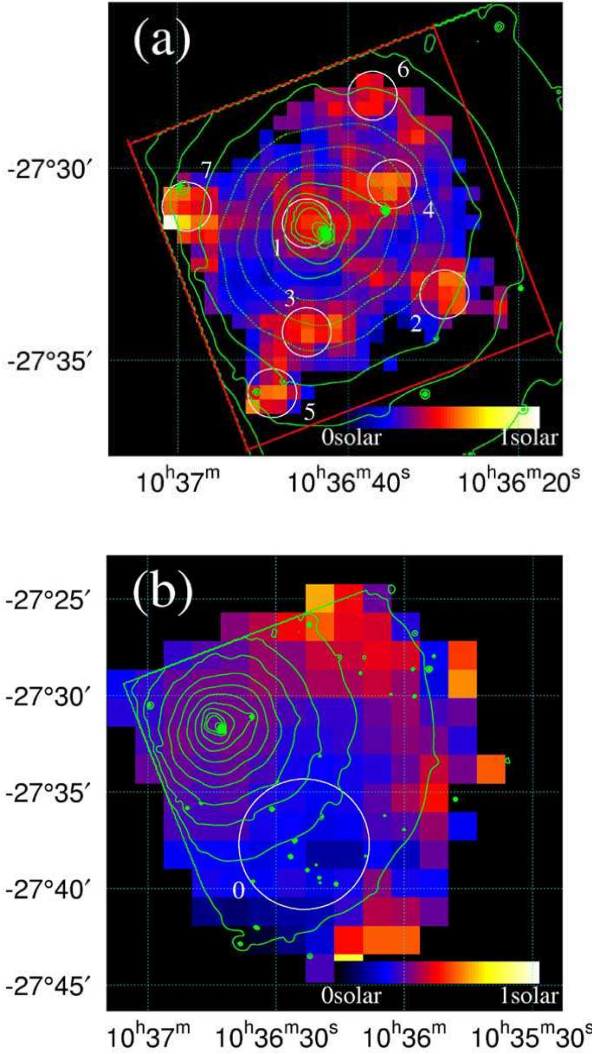


Fig. 7. (a) Distribution of the iron-band hardness ratios, smoothed in $22'' \times 22''$ pixels (5 kpc across). Results for only ACIS-I3 chip (indicated with red square) are shown. Several high-abundance regions are encircled and numbered. The contours indicate the X-ray intensity. (b) Same distribution as in (a), but the data were smoothed in $88'' \times 88''$ pixels (20 kpc across) to show a larger scale distribution. The extended low-abundance region is numbered as 0 and encircled.

6. High Metallicity Regions

As shown in the previous section, there are several high-metallicity regions near the center of the A 1060 cluster. Here, we evaluate their properties based on the spectral fit. The pulse-height data were accumulated separately for the 8 regions indicated in figures 7a and b, and spectral fits were performed. Table 1 summarizes the fit, and the results are plotted in figure 9. Data #0 is the extended low-abundance region, and #1-7 are the high-abundance ones. The errors are single-parameter 90% limits (1.65σ). Compared with the #0 level, most of the regions indicate deviations by less than 2σ , and the significances are rather low. Only region #1 shows a 3.4σ deviation, which

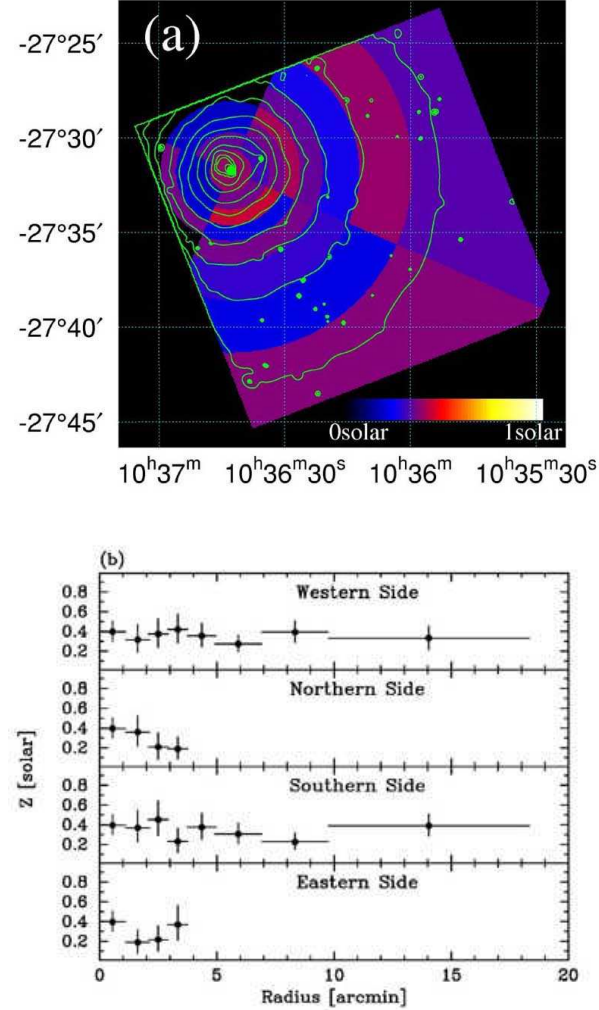


Fig. 8. (a) Spatial distribution of metal abundance based on spectral fits. (b) Radial abundance profiles for 4 directions, obtained from the spectral fits as shown in panel a.

strongly suggests that Fe is concentrated in this small region with a diameter less than 10 kpc. We refer to this region as “metal-rich blob” hereafter. We also note that the temperature of regions #1 is not significantly different from that of the surrounding level.

Table 1. Results of spectral fits for selected regions in figure 7.

Region (#)	kT (keV)	Z (solar)	F_X ($\text{erg cm}^{-2}\text{s}^{-1}$)	L_X (erg s^{-1})
0	$2.95^{+0.12}_{-0.09}$	$0.26^{+0.05}_{-0.06}$	$6.90^{+0.07}_{-0.11} \times 10^{-12}$	$1.73^{+0.02}_{-0.03} \times 10^{42}$
1	$3.55^{+0.25}_{-0.25}$	$0.74^{+0.29}_{-0.23}$	$1.10^{+0.05}_{-0.07} \times 10^{-12}$	$2.75^{+0.01}_{-0.02} \times 10^{41}$
2	$3.51^{+0.57}_{-0.48}$	$0.44^{+0.53}_{-0.31}$	$4.46^{+0.29}_{-0.49} \times 10^{-13}$	$1.12^{+0.07}_{-0.12} \times 10^{41}$
3	$3.85^{+0.48}_{-0.37}$	$0.77^{+0.50}_{-0.46}$	$6.40^{+0.14}_{-0.72} \times 10^{-13}$	$1.60^{+0.09}_{-0.18} \times 10^{41}$
4	$3.70^{+0.37}_{-0.41}$	$0.29^{+0.31}_{-0.21}$	$7.07^{+0.37}_{-0.53} \times 10^{-13}$	$1.77^{+0.13}_{-0.63} \times 10^{41}$
5	$3.20^{+1.84}_{-0.77}$	$0.44^{+0.32}_{-0.42}$	$1.60^{+0.25}_{-0.81} \times 10^{-13}$	$4.00^{+0.63}_{-0.70} \times 10^{40}$
6	$4.00^{+0.65}_{-0.71}$	$0.38^{+0.48}_{-0.31}$	$2.58^{+0.28}_{-0.49} \times 10^{-13}$	$6.46^{+0.70}_{-1.23} \times 10^{40}$
7	$3.66^{+1.06}_{-0.72}$	$0.65^{+1.68}_{-0.52}$	$4.46^{+0.23}_{-0.46} \times 10^{-13}$	$1.12^{+0.06}_{-0.12} \times 10^{41}$

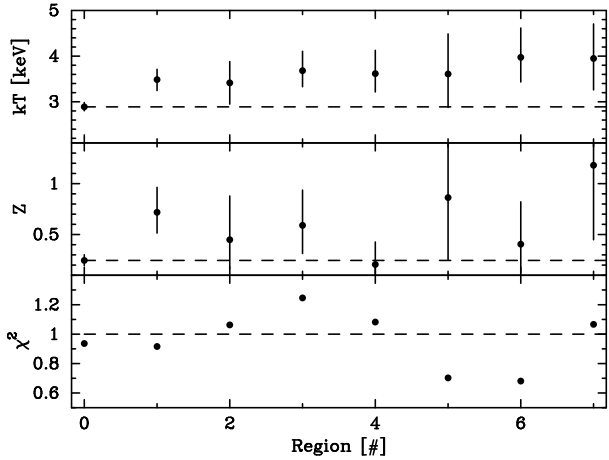


Fig. 9. Temperature and metal abundance obtained from spectral fits for the regions marked in figures 7a and b. The errors are single-parameter 90% limits.

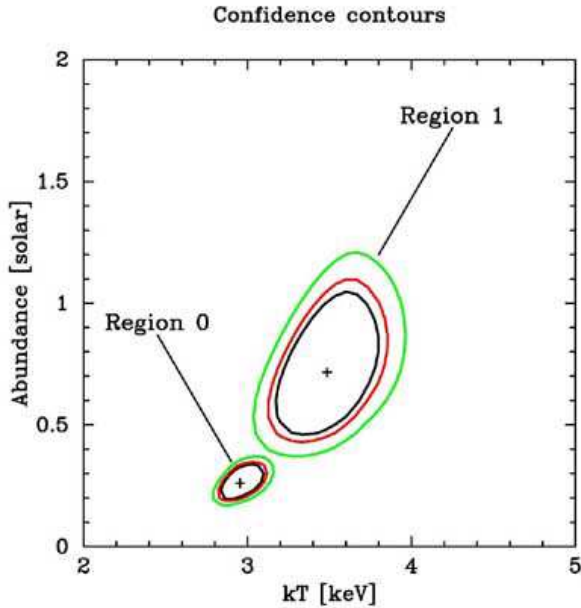


Fig. 10. Confidence contours for the spectral parameters for the pulse-height spectra of regions #0 and #1. The confidence levels are 90% (black), 95% (red), and 99% (green) for 2 interesting parameters. The two spectra have different abundance at more than the 99% confidence level.

To make a close spectral comparison between regions #0 and #1, we show confidence contours of the fit in figure 10. The metal abundance in #1 is 0.74 solar, which is about 3 times higher than the #0 level of 0.26 solar. The #1 temperature is higher than #0 by 0.5 keV, but about the same as in the surrounding regions. The 2-dimensional confidence contours indicate that these 2 spectra have a different abundance at the 99% confidence level.

To compare with the iron abundance feature, we consider the optical galaxy distribution, which is shown in figure 2a. The abundance enhancement around the north of NGC 3311 may be related to this galaxy (or an internal

structure of the galaxy), since the isophotal radius of NGC 3311 ($r_e = 95''$) is outside of the high-abundance region. Another iron concentration is seen at 3' to the southwest of the cluster center ($RA \simeq 10^h 36^m 28^s$, $Dec \simeq -27^\circ 33'$). However, no galaxies are seen in the optical image. These features indicate that the iron enhancement does not generally occur at the positions of the present bright galaxies. This suggests that the injection of iron into the ICM may have occurred in the past when the galaxy positions and brightnesses were much different from the present configuration.

7. Discussion

The present analysis on the Chandra data of A 1060 confirmed the absence of a central cool component with high spatial resolution. At the same time, there are significant inhomogeneities in the spatial distributions of the temperature and metallicity. We discuss their implications in this section.

7.1. Temperature Distribution

First, let us briefly examine the temperature structure. The radial temperature profile shows a peak at around ~ 35 kpc ($\sim 160''$) from the center with a level 20% higher than that of the outer region, accompanied by a gradual decline toward the center. The temperature maps and the profiles in 4 directions (figures 5 and 6) indicate that this high-temperature region is encircling the central region ($r < 5'$) with no sharp difference in the azimuthal directions. Previous ASCA observations did not have the necessary spatial resolution to resolve these features (Tamura et al. 2000; Furusho et al. 2001).

Numerical simulations of cluster formation generally predict a fairly steep temperature drop toward the outer regions (Frenk et al. 1999), with a factor of 2 drop at a radius of $\sim 0.5 r_{180}$. Here, r_{180} is the radius within which the mean density is 180 times the critical density, and the matter is approximately virialized within this radius. For A 1060, $r_{180} \approx 1.5$ Mpc, which is 20 times larger than the radius for the observed temperature drop. Therefore, the “hot ring” is likely to be caused by a process taking place only in the central region. Since the ICM temperature is fairly constant at 3.0 keV for $r = 8' - 30'$ as shown by the present data and the previous ASCA results (Furusho et al. 2001), we should think that extra energy is carried in within the central 50 kpc.

A 1060 has 2 bright central galaxies, NGC 3311 and NGC 3309, near the center, separated by 22 kpc in projection. This suggests that A 1060 may have gone through a merger in the long past, with the above 2 galaxies located at the centers of each component. During the merger, the central galaxies may have lost a large portion of the halo gas, but the stellar component would have remained. This can explain the observed very compact X-ray halos of these 2 galaxies (Yamasaki et al. 2002). Since the 3-dimensional distance between the 2 galaxies should be larger than 22 kpc, the diameter of the “hot ring” is comparable to the region covered by the motions of the central

galaxies. However, it is not obvious how extra energies were created in this region. Merger should create a temperature structure, such as that seen in the double-core cluster, A 2256. However, because the ICM of A 1060 is much more isothermal, the temperature variation directly caused by the merger is likely to have already been smoothed out.

One possibility that we consider here is the energy input from bright galaxies. Supernova and stellar winds in the galaxies can inject a significant amount of heat into the surrounding ICM in the form of galactic winds. We can perform a crude estimation by considering only the supernova effects. Based on the supernova rate, $(0.16 \pm 0.06) \times 10^{-12} \text{ yr}^{-1} L_{B\odot}^{-1}$, given by Cappellaro et al. (1999), the total supernova rate in the 2 elliptical galaxies ($L_B \approx 1.9 \times 10^{11} L_\odot$) is estimated to be $\sim 0.03 \text{ yr}^{-1}$. Assuming that each supernovae gives an energy of 10^{51} erg, the total energy input is 3×10^{58} erg in 10^9 yr , which is roughly 20% of the thermal energy contained in a volume with the radius of 25 kpc in the cluster center. This estimation suggests that, over a time scale of 10^9 yr , energy input from galaxies can make a significant contribution to the thermal structure of the ICM. We, however, note that because the central galaxies contain cool gas compared with the ICM (Yamasaki et al. 2002), either a high galaxy motion or a wind-like mass ejection would be necessary to heat the surrounding ICM efficiently.

The slight drop of temperature at the center may be explained by cooling. The radiative cooling time at the center of A 1060 is estimated to be $6.6 \times 10^9 \text{ yr}$, which is comparable to the Hubble time ($1.3 \times 10^{10} \text{ yr}$), and much longer than the heat conduction time shown below. Therefore, radiative cooling at the cluster center is not a dominant effect. The heat-conduction time scale can be calculated from the central density and core radius given by the β -model fit. The conduction time at the cluster center is estimated to be $1.4 \times 10^9 \text{ yr}$, which is ten times shorter than the Hubble time. The observed isothermality, better than most of other clusters, in the central region of A 1060 suggest that the heat conduction is working at the theoretical level, and that the suppressing effect, such as due to a magnetic field, is small.

7.2. Mass Distribution

Based on an approximation of constant temperature and metallicity as well as spherical symmetry, we have derived the density distribution in a model-independent way. Compared with the simple β model that can fit the data at $r > 4'$, the central gas density is about twice higher, as shown in figure 4. If the ICM is in hydrostatic equilibrium, the observed high density of the gas simply indicates a concentration of the gravitational mass. Assuming an isothermality for simplicity, we have derived a gravitational mass profile, which is shown along with the gas mass profile in figure 11a. The corresponding mass density profiles are also shown in figure 11b. In these figures, the mass profiles for a simple β model are plotted for a comparison. We notice an excess in the central region within $r = 50 \text{ kpc}$ over the simple β profile, and the gravi-

tational mass is about 5 times higher in the central 10 kpc. Since this feature may have resulted due to our neglect of the temperature variation shown in figure 3, we also plot a mass curve including the temperature variation. The results are shown by diamonds in figures 11a and b.

Tamura et al. (2000) showed, based on the analyses of the ASCA and ROSAT data of A 1060, that the mass profile is well described by a NFW profile (Navarro et al. 1997) with a central slope ~ 1.5 . Their analyses, however, did not exclude the compact halo of NGC 3311, which may have acted in favor of the cusp-like central structure.

The present result confirms that there is a significant concentration of dark matter in the central 50 kpc region, and that baryons (gas and galaxies) do not simply follow this feature. In fact, the radial profile of the baryon fraction shows a marked drop at the center. Ota and Mitsuda (2002) reported, based on the analysis of 79 cluster data obtained by ROSAT, a double-peak distribution for the core radius with peaks at 60 kpc and 220 kpc. Therefore, these observed results jointly suggest that dark matter may preferentially be accumulated within a radius of 50–60 kpc.

7.3. Metal Distribution

The Chandra data confirmed that the radial distribution of the metal abundance is fairly uniform with an average value of ~ 0.3 solar, which agrees with the previous results (Tamura et al. 1996). Recent Chandra and XMM-Newton observations have revealed that in several clusters of galaxies the radial metal abundance profile shows a peak offset from the center. Furusho et al. (2003) found that, in the poor cluster AWM 7, this feature is mainly caused by two high-metallicity blobs symmetrically placed around the center. The radial metallicity distribution in A 1060 seems to be more uniform than that of the above clusters. Morris and Fabian (2003) discussed that some abundance profile may be related to the evolution and metallicity of the central cool component. The flat radial distribution of metallicity in A 1060 suggests that this cluster is still in an early phase of evolution.

The present Chandra observation showed that the iron distribution in the central region of A 1060 is not completely uniform. Several local concentrations with roughly arcminute scales ($1'$ or 13 kpc) are recognized, with no spatial correspondence with the bright galaxies. We here examine the origin of iron in the ICM and the history of metal injection.

Let us first estimate the mass of iron in the high-metallicity region. We consider only the region at the northeast of NGC 3311, since it is the brightest and the most significant among the high-metallicity regions. Because the measured abundance is $0.74^{+0.29}_{-0.23}$ solar for the projected data, the true abundance of the high-metallicity region must be significantly higher. For this estimation, we need to subtract the foreground and background components of the ICM in the line of sight. We employ our density profile shown in figure 4, which gives the gas density at 10 kpc from the cluster center to be $7.6 \times 10^{-3} \text{ cm}^{-3}$.

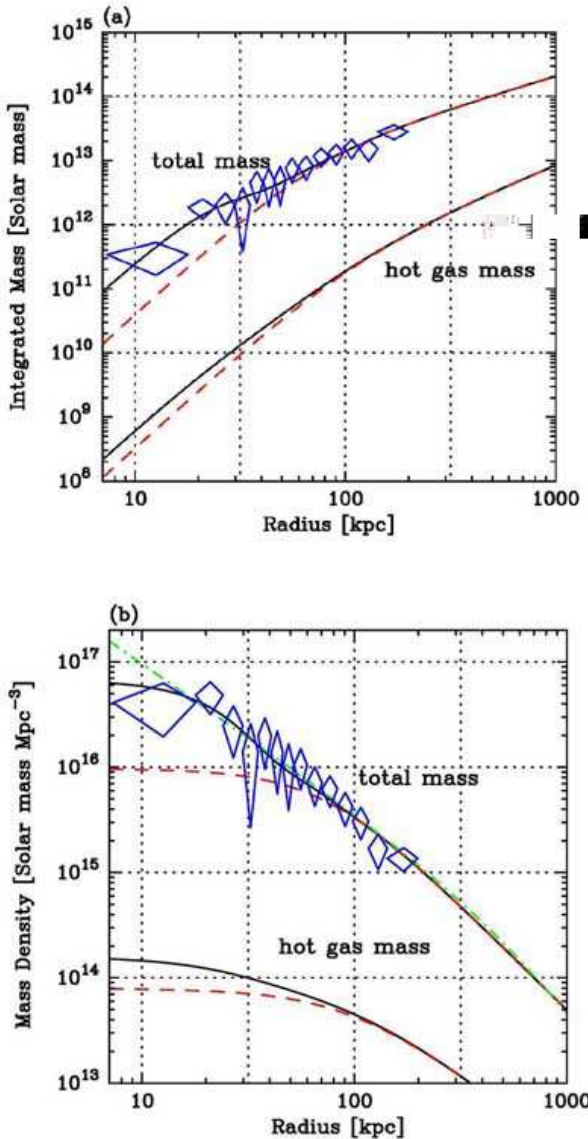


Fig. 11. (a) Gravitational mass profile estimated from the simple β -model (upper dashed line) and the density profile shown in figure 4 (upper solid line). The lower lines represent the ICM mass based on the β -model and the density profile in figure 4, respectively. The diamonds show the results when the temperature variation shown in figure 3 is considered. (b) Same as (a), but for the differential mass density profiles. The dash-dotted line shows a NFW model with a central density slope of 1.5.

Since the metal-rich region is more luminous than the ambient region at the same distance from the cluster center, it must have a higher density. In the later estimation of the physical parameters, we simply approximate that the region has a spherical blob shape with a radius of 8.7 kpc (40'') filled with a constant gas density. The measured value of the excess luminosity, $L_X = 2.75^{+0.01}_{-0.02} \times 10^{41}$ erg s $^{-1}$, gives the gas density to be about 1.1×10^{-2} cm $^{-3}$ and the blob mass about $7 \times 10^8 M_\odot$. We note that the derived blob mass is larger than that of the compact X-ray

halo of NGC 3311, which is estimated to be $5.6 \times 10^7 M_\odot$ (Yamasaki et al. 2002). The spectral fit indicates that the metal abundance of the blob region is ~ 0.7 solar. Again, this is a “diluted” value, since the data contain all of the emission in the line of sight. We corrected for the projected effect, assuming the same density distribution. The metal abundance of the blob is found to be 1.5 solar, which is 4–5 times higher than the average cluster value.

Based on these results, the total mass of Fe (M_{Fe}) contained in the blob is estimated to be $3.0 \times 10^6 M_\odot$. The question is whether this much Fe can be supplied by a single galaxy, NGC 3311. The stellar mass of NGC 3311 is estimated to be $4.8 \times 10^{11} M_\odot$, assuming $M/L_B = 8.5 (M_\odot/L_\odot)$ and $L_B = 11.15$ (Faber et al. 1989). The X-ray halo of NGC 3311 gives a negligible contribution. If the average Fe abundance in the stellar mass is 1 solar, we obtain $M_{\text{Fe}} \sim 1.3 \times 10^9 M_\odot$ as the total stellar Fe content. The above-estimated M_{Fe} in the blob is only 0.2% of the stellar Fe content, and can be supplied by a single galaxy. The metal-rich blob can possibly be a stripped halo of NGC 3311, as far as the gas mass and Fe content are concerned.

To further examine the consistency of this picture, we estimate the ram pressure stripping time for a galaxy moving in the ICM based on the following formula (Sarazin 1988):

$$t \sim 3.0 \times 10^7 \left(\frac{\rho_{\text{ISM}}}{\rho_{\text{ICM}}} \right)^{1/2} \left(\frac{v}{10^3 \text{ km s}^{-1}} \right)^{-1} \left(\frac{R}{10 \text{ kpc}} \right) \text{ yr}$$

Taking $\rho_{\text{ISM}}/\rho_{\text{ICM}} \approx 10$, $v \approx 500 \text{ km s}^{-1}$, and $R \approx 2 \text{ kpc}$ (Yamasaki et al. 2002), the stripping time was estimated to be about $1.0 \times 10^7 \text{ yr}$. The galaxy can travel about 6 kpc within the stripping time, which is about the same distance from NGC 3311 to the blob center. Based on these supporting features, we consider that the metal-rich blob is likely to be the gas stripped off from NGC 3311.

Except for these blob-like metal concentrations, the general cluster space seems to show a fairly uniform metal abundance. Therefore, we need to understand how metals are eventually mixed into the general ICM space. As pointed out by several authors (Metzler and Evrard 1994; Ezawa et al. 1997), the diffusion of Fe in the ICM is very slow, and mixing due to galaxy motions or to subcluster mergers would be necessary. We hope that future observational and theoretical studies will give us a comprehensive view on the metal enrichment process. An XMM-Newton observation of A 1060 will soon reveal the metal distribution and temperature structure in more detail with its larger collecting area.

8. Conclusion

A Chandra observation of the A 1060 cluster confirmed that the temperature and metal abundance distributions are fairly uniform from the outer region ($r \sim 230 \text{ kpc}$) to the central 5 kpc region. Regarding the temperature, the radial profile shows a broad peak at around 35 kpc from the center at a level 20% higher than that of the outer

region. This may reflect the condition of the hydrostatic equilibrium as numerical simulations suggest. These results suggest that this cluster is relaxed, and has a relatively slow growth speed of its evolution. Assuming a constant temperature and metal abundance, we derived a 3-dimensional density profile by iteration on the initial β model. The gas distribution implies a concentration of gravitational matter within a radius of 50 kpc. For metal abundance, we detected several metal-rich regions around the central region. In particular, the central blob adjacent to the galaxy NGC 3311 exhibits a high abundance (1.5 solar) and gas density ($1.1 \times 10^{-2} \text{ cm}^{-3}$). We interpret this to be caused by gas-stripping from NGC 3311.

T.F. acknowledges support from the Japan Society for the Promotion of Science. This work was partly supported by the Grants-in-Aid for Scientific Research No. 14079103 from the Ministry of Education, Culture, Sports, Science and Technology, and No. 15340088 from the Japan Society for the Promotion of Science.

References

Anders, E., & Grevesse, N. 1989, *Geochim. Cosmochim. Acta* 53, 197

Blanton, E. L., Sarazin, C. L., & McNamara, B. R. 2003, *ApJ*, 585, 227

Böhringer, H., Matsushita, K., Churazov, E., Finoguenov, A., & Ikebe, Y. 2004, *A&A*, 416, L21

Cappellaro, E., Evans, R., & Turatto, M. 1999, *A&A*, 351, 459

De Grandi, S., Ettori, S., Longhetti, M., & Molendi, S. 2004, *A&A*, 419, 7

Edge, A. C., & Stewart, G. C. 1991, *MNRAS*, 252, 414

Ezawa, H., Fukazawa, Y., Makishima, K., Ohashi, T., Takahara, F., Xu, H., & Yamasaki, N. Y. 1997, *ApJ*, 490, L33

Faber, S. M., Wegner, G., Burstein, D., Davies, R. L., Dressler, A., Lynden-Bell, D., & Terlevich, R. J. 1989, *ApJS*, 69, 763

Frenk, C. S., et al. 1999, *ApJ*, 525, 554

Fukazawa, Y., Makishima, K., Tamura, T., Ezawa, H., Xu, H., Ikebe, Y., Kikuchi, K., & Ohashi, T. 1998, *PASJ*, 50, 187

Furusho, T., et al. 2001, *PASJ*, 53, 421

Furusho, T., Yamasaki, N. Y., & Ohashi, T. 2002, in *Proc. New Visions of the X-ray Universe in the XMM-Newton and Chandra Era* (ESTEC) in press (astro-ph/0203244)

Furusho, T., Yamasaki, N. Y., & Ohashi, T. 2003, *ApJ*, 596, 181

Ikebe, Y., et al. 1996, *Nature*, 379, 427

Iwasawa, K., Fabian, A. C., Allen, S. W., & Ettori, S. 2001, *MNRAS*, 328, L5

Johnstone, R. M., Allen, S. W., Fabian, A. C., & Sanders, J. S. 2002, *MNRAS*, 336, 299

Matsushita, K., Makishima, K., Ikebe, Y., Rokutanda, E., Yamasaki, N., & Ohashi, T. 1998, *ApJL*, 499, L13

Mazzotta, P., Edge, A. C., & Markevitch, M. 2003, *ApJ*, 596, 190

Metzler, C. A., & Evrard, A. E. 1994, *ApJ*, 437, 564

Molendi, S., & Gastaldello, F. 2001, *A&A*, 375, L14

Morris, R. G., & Fabian, A. C. 2003, *MNRAS*, 338, 824

Navarro, J. F., Frenk, C. S., & White, S. D. M. 1997, *ApJ*, 490, 493

Ota, N., & Mitsuda, K. 2002, *ApJ*, 567, L23

Peterson, J. R., Kahn, S. M., Paerels, F. B. S., Kaastra, J. S., Tamura, T., Bleeker, J. A. M., Ferrigno, C., & Jernigan, J. G. 2003, *ApJ*, 590, 207

Sanders, J. S., & Fabian, A. C. 2002, *MNRAS*, 331, 273

Sanders, J. S., Fabian, A. C., Allen S. W., & Schmidt, R. W. 2004, *MNRAS*, 349, 952

Sarazin, C. L. 1988, *X-ray emission from clusters of galaxies*, (Cambridge: Cambridge University Press)

Schmidt, R. W., Fabian, A. C., & Sanders, J. S. 2002, *MNRAS*, 337, 71

Tamura, T., et al. 1996, *PASJ*, 48, 671

Tamura, T., Makishima, K., Fukazawa, Y., Ikebe, Y., & Xu, H. 2000, *ApJ*, 535, 602

Tanaka, T., Hudaverdi, M., Akimoto, F., Furuzawa, A., Tawara, Y., & Yamashita, K. 2003, *Proc. Workshop on Galaxies and Clusters of Galaxies* (Tokyo: Japan Society for the Promotion of Science), 99

Yamasaki, N. Y., Ohashi, T., & Furusho, T. 2002, *ApJ*, 578, 833